The influence of quantum degeneracy and irreversibility on the performance of a Fermi quantum refrigeration cycle



2004 J. Phys. A: Math. Gen. 37 7485

(http://iopscience.iop.org/0305-4470/37/30/007)

INSTITUTE OF PHYSICS PUBLISHING JOURNAL OF PHYSICS A: MATHEMATICAL AND GENERAL

J. Phys. A: Math. Gen. **37** (2004) 7485–7497 PII: S0305-4470(04)75361-5

# The influence of quantum degeneracy and irreversibility on the performance of a Fermi quantum refrigeration cycle

**Yue Zhang**[1], **Bihong Lin**[1,2] **and Jincan Chen**[1]

[1] Department of Physics, Xiamen University, Xiamen 361005, People's Republic of China
[2] Department of Physics, Quanzhou Normal University, Quanzhou 362000, People's Republic of China

E-mail: jcchen@xmu.edu.cn

Received 29 January 2004, in final form 3 June 2004
Published 14 July 2004
Online at stacks.iop.org/JPhysA/37/7485
doi:10.1088/0305-4470/37/30/007

**Abstract**

An irreversible cycle model of the quantum refrigeration cycle using an ideal Fermi gas as the working substance is established. The cycle consists of two adiabatic and two isobaric processes and consequently may be simply referred to as the Fermi Brayton refrigeration cycle. The performance of the cycle is investigated, based on the equation of state of an ideal Fermi gas. Expressions for several important performance parameters, such as the coefficient of performance, work input and refrigeration load, are derived. The influence of the quantum degeneracy of the Fermi gas and the irreversibility in the cycle on the performance of the Fermi Brayton refrigeration cycle is analysed. The minimum pressure ratio of the cycle is determined. The optimally operating problems of the cycle and several special cases are discussed in detail. The results obtained here are general and may reveal the general performance characteristics of the Fermi Brayton refrigeration cycle.

PACS numbers: 05.70.−a, 07.20.Mc, 44.90.+c

## 1. Introduction

The classical ideal gas equation of state is one of the important equations of classical thermodynamics. It has been widely used to analyse the performance of thermodynamic cycles. However, when the temperature of the gas is low enough or its density is high enough, the gas will deviate from its classical behaviour and the quantum degeneracy of the gas becomes important [1–3]. Under these conditions, the gases obey Bose–Einstein or Fermi–Dirac statistics and are called ideal quantum gases. Obviously, the performance of the

  

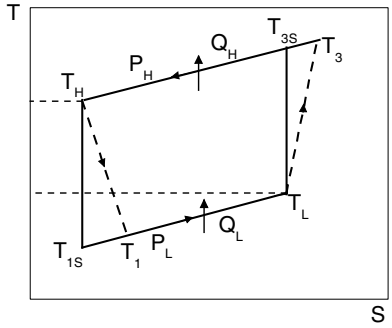


**Figure 1.** The temperature–entropy diagram of an irreversible Brayton refrigeration cycle.

cycle using an ideal quantum gas as the working substance is different from one of the cycles working with a classical ideal gas. Thus, the performance analysis of quantum thermodynamic cycles has become an interesting research subject [2–9].

In recent years, several authors have investigated, respectively, the performance of quantum refrigeration [2, 6, 7, 9] and power cycles [4, 5, 8] using the Bose or Fermi gases as the working substance and many meaningful conclusions have been obtained. However, these investigations are mainly concentrated on the influence of the quantum degeneracy on the performance of reversible thermodynamic cycles working with quantum gases, while the influence of the irreversibility in the quantum gas thermodynamic cycle has rarely been considered. Practical cycles are always irreversible. In order to understand more deeply the performance of a quantum refrigeration cycle, we will investigate the influence of both the quantum degeneracy of the gas and the irreversibility of the cycle on the performance of a quantum Brayton refrigeration cycle working with an ideal Fermi gas in this paper. It can be expected that some more general and useful results, which may reveal the performance characteristics of an irreversible Fermi quantum Brayton refrigeration cycle, are obtained.

## 2. An irreversible quantum refrigeration cycle

A Brayton refrigeration cycle using an ideal Fermi gas as the working substance is composed of two adiabatic and two isobaric processes. Figure 1 shows the temperature–entropy diagram of the cycle, where the two nearly vertical dashed lines indicate two irreversible adiabatic processes, $P_H$ and $P_L$ are the pressures of the high and low constant-pressure processes, $Q_H$ and $Q_L$ are the amounts of heat exchanged between the working substance and the heat reservoirs at temperature $T_H$ and $T_L$ during the two constant-pressure processes, $T_{1S}$ and $T_{3S}$ are the final temperatures of the reversible adiabatic expansion and compression processes, and $T_1$ and $T_3$ are the final temperatures of the irreversible adiabatic expansion and compression processes. It should be pointed out that $T_H$ and $T_L$ are also the temperatures of the working substance at the beginning of the expansion and compression processes, because the irreversibility of heat transfer between the working substance and the external heat reservoirs has not been taken into account in this cycle model.

In the performance analysis of a Brayton refrigeration cycle, it will be significant to discuss the influence of irreversibility in the working substance because the processes in a real cycle are always irreversible. According to figure 1, we may introduce the compression and expansion efficiencies [10–13]

$$\eta_c = \frac{T_{3S} - T_L}{T_3 - T_L} \tag{1}$$

and

$$\eta_e = \frac{T_H - T_1}{T_H - T_{1S}} \tag{2}$$

to describe the irreversibility of the cycle. When $\eta_c = 1$ and $\eta_e = 1$, the compression and expansion processes become reversible. It is clear that the cycle model established here is more general, so that the reversible model of the Brayton refrigeration cycle is only a special case of the present model.

## 3. Several important parameters

In order to obtain the expressions for several important parameters of the cycle, we first calculate the heat capacity $C_P$ at constant pressure of an ideal Fermi gas. According to statistical mechanics, the expressions of the pressure, number density, internal energy and entropy for an ideal Fermi gas are given by [14, 15]

$$P = \frac{gkT}{\lambda^3} f_{5/2}(z) = nkT F(z), \tag{3}$$

$$n = \frac{N}{V} = \frac{g}{\lambda^3} f_{3/2}(z), \tag{4}$$

$$U = \frac{3}{2} NkT F(z) \tag{5}$$

and

$$S = Nk\left[\tfrac{5}{2}F(z) - \ln(z)\right], \tag{6}$$

respectively, where $k$ is the Boltzmann constant, $g$ is a weight factor that arises from the 'internal structure' of particles (in this paper, we adopt $g = 1$), $T$, $N$ and $V$ are, respectively, the gas temperature, total number of particles and volume, $z = \mathrm{e}^{\beta\mu}$ and $\lambda = h/(2\pi mkT)^{1/2}$ are, respectively, the fugacity of the gas and the mean thermal wavelength of particles, $\beta = 1/(kT)$, $\mu$ is the chemical potential of the gas, $h$ is Planck's constant, $m$ is the rest mass of a particle, $f_l(z) = \frac{1}{\Gamma(l)} \int_0^\infty \frac{x^{l-1}}{z^{-1}\mathrm{e}^x + 1}\,\mathrm{d}x$ is called the Fermi function, $\Gamma(l)$ is the Gamma function, and $F(z) = f_{5/2}(z)/f_{3/2}(z)$ can be called the correction function. When $F(z) = 1$, an ideal Fermi gas becomes an ideal classical gas. Using equations (3)–(6), the heat capacities at constant volume and at constant pressure can be, respectively, expressed as

$$C_V = \frac{15}{4} Nk \frac{f_{5/2}(z)}{f_{3/2}(z)} - \frac{9}{4} Nk \frac{f_{3/2}(z)}{f_{1/2}(z)} = \frac{3}{2} Nk \frac{\mathrm{d}}{\mathrm{d}T}[T F(T, P)] \tag{7}$$

and

$$C_P = C_V + T\left(\frac{\partial P}{\partial T}\right)_V \left(\frac{\partial V}{\partial T}\right)_P = \frac{5}{2} Nk \frac{\mathrm{d}}{\mathrm{d}T}[T F(T, P)], \tag{8}$$

where $F(T, P)$ is a function of temperature and pressure.

On the other hand, for an ideal Fermi gas, the ratio of the entropy $S$ of the system to the total number of particles $N$ is only a function of the ratio of the chemical potential $\mu$ to temperature $T$, i.e. $S/N = \varphi(\mu/T)$. During an isentropic process, the values of $\mu/T$ and $z$ remain unchanged because $S$ and $N$ are unchanged [15]. Using the property of the isentropic processes and equation (6), one can obtain

$$F(P_L, T_L) = F(P_H, T_{3S}), \qquad F(P_L, T_{1S}) = F(P_H, T_H). \tag{9}$$

Using equation (3) again, one can obtain

$$\frac{T_{3S}}{T_L} = \frac{T_H}{T_{1S}} = \left(\frac{P_H}{P_L}\right)^{2/5} = r_P^{2/5}, \tag{10}$$

where $r_P = P_H/P_L$ is the pressure ratio of two constant-pressure processes. From equations (1), (2) and (10), one can further obtain

$$T_1 = T_H\left[1 - \eta_e\left(1 - 1/r_P^{2/5}\right)\right] = T_H X, \qquad T_3 = T_L\left[1 + \left(r_P^{2/5} - 1\right)/\eta_c\right] = T_L Y, \tag{11}$$

where $X = 1 - \eta_e\left(1 - 1/r_P^{2/5}\right)$ and $Y = 1 + \left(r_P^{2/5} - 1\right)/\eta_c$.

Using equations (8) and (11), one can find that the amounts of heat exchanged in the two constant-pressure processes mentioned above are, respectively, given by

$$Q_H = \int_{T_H}^{T_3} C_P \,\mathrm{d}T = \frac{5}{2}Nk[T_L Y F(T_L Y, P_H) - T_H F(T_H, P_H)] \tag{12}$$

and

$$Q_L = \int_{T_1}^{T_L} C_P \,\mathrm{d}T = \frac{5}{2}Nk[T_L F(T_L, P_L) - T_H X F(T_H X, P_L)]. \tag{13}$$

For a Brayton refrigeration cycle, the refrigeration load is determined by equation (13), while work input, $W$, of the cycle and the coefficient of performance (COP), $\varepsilon$, are expressed as

$$W = Q_H - Q_L = \tfrac{5}{2}NkT_H[\tau Y F(T_L Y, P_H) - F(T_H, P_H) - \tau F(T_L, P_L) + X F(T_H X, P_L)] \tag{14}$$

and

$$\varepsilon = \frac{Q_L}{W} = \frac{\tau F(T_L, P_L) - X F(T_H X, P_L)}{\tau Y F(T_L Y, P_H) - F(T_H, P_H) - \tau F(T_L, P_L) + X F(T_H X, P_L)}, \tag{15}$$

respectively, where $\tau = T_L/T_H$ is the temperature ratio of two heat reservoirs. Equations (13)–(15) show that the refrigeration load, work input and COP of the cycle are functions of the temperatures of the heat reservoirs, pressures of the constant-pressure processes and compression and expansion efficiencies. Starting from these equations, we can discuss the performance of a Fermi Brayton refrigeration cycle.

In addition, in order to compare the performance of an irreversible quantum Brayton refrigeration cycle with that of an irreversible classical Brayton refrigeration cycle using an ideal gas as the working substance, we introduced a relative refrigeration load as

$$R_{\mathrm{QL}} = \frac{Q_L}{Q_L^C} = \frac{\tau F(T_L, P_L) - X F(T_H X, P_L)}{\tau - X}, \tag{16}$$

where $Q_L^C = \frac{5}{2}NkT_H(\tau - X)$ is the refrigeration load of an irreversible classical Brayton refrigeration cycle using an ideal gas as the working substance and will be given in equation (32). It should be noted that equations (13) and (16) and other equations derived from the two equations are independent of the compression efficiency.

## 4. Performance characteristics

Using equations (13)–(16) and assuming $^3$He as the working substance, one can generate the $Q_L^* \sim r_P$, $W^* \sim r_P$, $\varepsilon \sim r_P$, $\varepsilon \sim Q_L^*$ and $R_{\mathrm{QL}} \sim r_P$ characteristic curves of the cycle for a set of given parameters ($T_L = 5$ K, $\tau = 0.25$, $P_L = 0.5$ MPa), as shown in figures 2–6, where $Q_L^* = 2Q_L/(5NkT_H)$ and $W^* = 2W/(5NkT_H)$ are, respectively, the dimensionless

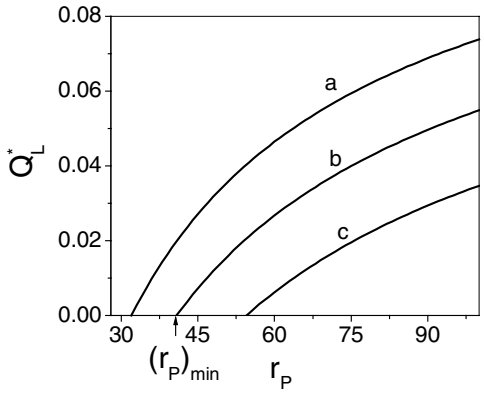


**Figure 2.** The $Q_L^*$–$r_P$ curves, where $Q_L^* = 2Q_L/(5NkT_H)$ is the dimensionless refrigeration load and the parameters $T_L = 5\,\mathrm{K}$, $T_H = 20\,\mathrm{K}$ and $P_L = 0.5\,\mathrm{MPa}$ are adopted. Curves a, b and c correspond to the cases of $\eta_e = 1.00$, 0.97 and 0.94, respectively.

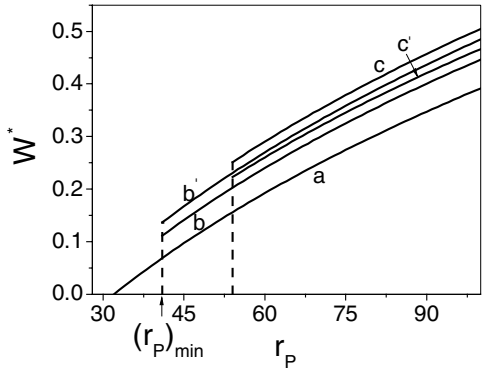


**Figure 3.** The $W^*$–$r_P$ curves, where $W^* = 2W/(5NkT_H)$ is the dimensionless work input. The values of the parameters $T_L$, $T_H$ and $P_L$ are the same as those used in figure 2. Curves a, b, c, b′ and c′ correspond to the cases of $\eta_e = \eta_c$ =1.00, 0.97, 0.94, $\eta_e = 0.97$ and $\eta_c = 0.94$, and $\eta_e = 0.94$ and $\eta_c = 0.97$, respectively.

refrigeration load and work input. Curves a, b, c, d, e, f, b′ and c′ correspond to the cases of $\eta_e = \eta_c = 1.00$, 0.97, 0.94, 0.999, 0.995, 0.99, $\eta_e = 0.97$ and $\eta_c = 0.94$, and $\eta_e = 0.94$ and $\eta_c = 0.97$, respectively.

It is clearly seen from figures 2 that when $r_P \leqslant (r_P)_{\min}$, the refrigeration load is smaller than or equal to zero and consequently the Brayton cycle cannot play a refrigeration role. Thus, the pressure ratio must satisfy the following relation:

$$r_P > (r_P)_{\min} \tag{17}$$

whose value is dependent on the temperatures of the heat reservoirs, pressures of the constant-pressure processes and expansion efficiencies and may be determined from equation (13), as listed in table 1. It is also seen from figure 2 that the minimum pressure ratio $(r_P)_{\min}$ increases as the irreversibility in the cycle increases.

Figure 3 clearly shows that the dimensionless work input $W^*$ is a monotonically increasing function of $r_P$ for given $T_L$, $T_H$, $P_L$, $\eta_e$ and $\eta_c$. Comparing figures 2 and 3, we can easily find that when $r_P = (r_P)_{\min}$, the refrigeration load is equal to zero while the work input is still

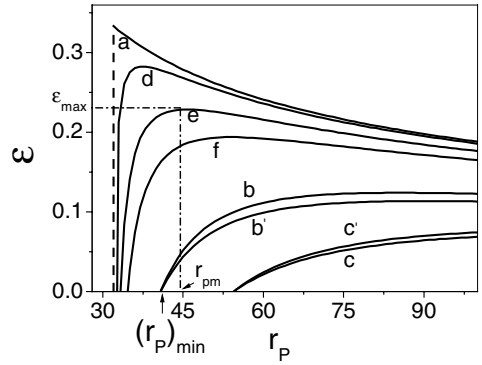


**Figure 4.** The $\varepsilon$–$r_P$ curves. The values of the parameters $T_L$, $T_H$ and $P_L$ are the same as those used in figure 2. Curves a, b, c, d, e, f, b′ and c′ correspond to the cases of $\eta_e = \eta_c$ =1.00, 0.97, 0.94, 0.999, 0.995, 0.99, $\eta_e = 0.97$ and $\eta_c = 0.94$, and $\eta_e = 0.94$ and $\eta_c = 0.97$, respectively.

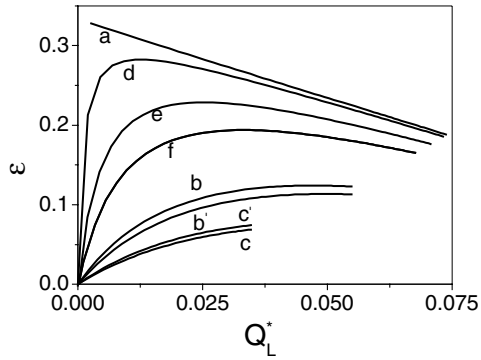


**Figure 5.** The $\varepsilon$–$Q_L^*$ curves. The values of the parameters $T_L$, $T_H$, $P_L$, $\eta_e$ and $\eta_c$ are the same as those used in figure 4.

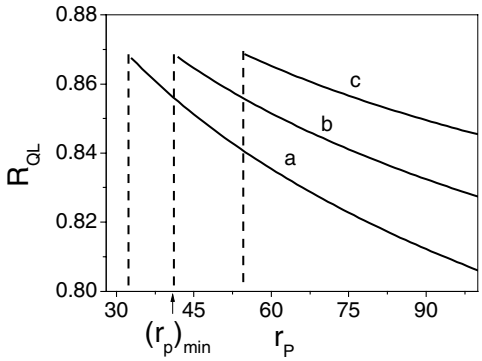


**Figure 6.** The $R_{\mathrm{QL}}$–$r_P$ curves. The values of the parameters $T_L$, $T_H$, $P_L$ and $\eta_e$ are the same as those used in figure 2.

larger than zero except for the special case when $\eta_e$ and $\eta_c$ are equal to 1. It is seen from the curves in figure 3 that the smaller the compression and expansion efficiencies are, the larger the work input. This implies that the work input increases with an increase in the irreversibility

**Table 1.** The minimum pressure ratio for different given parameters.

| $\eta_e$ | $\tau$ | $(r_P)_{\min}$ |
|---|---|---|
| 1.00 | 0.25 | 32.00 |
| | 0.35 | 13.80 |
| | 0.45 | 7.36 |
| | 0.55 | 4.46 |
| 0.99 | 0.25 | 34.56 |
| | 0.35 | 14.47 |
| | 0.45 | 7.60 |
| | 0.55 | 4.55 |
| 0.97 | 0.25 | 40.82 |
| | 0.35 | 16.00 |
| | 0.45 | 8.11 |
| | 0.55 | 4.75 |
| 0.94 | 0.25 | 54.44 |
| | 0.35 | 18.92 |
| | 0.45 | 9.02 |
| | 0.55 | 5.10 |

of the cycle. Obviously, the performance of the cycle can be improved by increasing the compression and expansion efficiencies. Moreover, comparing the curves b′ and c′ in figure 3, one can find that the influence of the compression efficiency on the work input is more obvious than that of the expansion efficiency.

It is clearly seen from the curves in figure 4 that for an irreversible Fermi Brayton refrigeration cycle, there exists an optimal value $r_{Pm}$ of the pressure ratio at which the coefficient of performance attains its maximum $\varepsilon_{\max}$, as shown in the curves b, b′, c, c′, d, e and f in figure 4; while for a reversible Fermi Brayton refrigeration cycle, the coefficient of performance decreases monotonically with the pressure ratio $r_P$, as shown in curve a in figure 4. The smaller the compression and expansion efficiencies are, the larger the pressure ratio $r_{Pm}$ at the maximum coefficient of performance. When the compression and expansion efficiencies are high and tend to 1, the corresponding pressure ratio $r_{Pm}$ is larger than $(r_P)_{\min}$, but close to $(r_P)_{\min}$. In such a case, when $\varepsilon < \varepsilon_{\max}$, there are two different pressure ratios for a given coefficient of performance $\varepsilon$, where one is smaller than $r_{Pm}$ and the other is larger than $r_{Pm}$. It is further seen from figures 4 and 5 that when $r_P < r_{Pm}$, the coefficient of performance decreases quickly as the refrigeration load decreases. It is thus clear that the region of $r_P < r_{Pm}$ is not reasonable for an irreversible Fermi quantum Brayton refrigeration cycle with high compression and expansion efficiencies. Consequently, the reasonable region of the pressure ratio should be

$$r_P > r_{Pm}. \tag{18}$$

This indicates that $r_{Pm}$ is an important parameter for an irreversible Fermi quantum Brayton refrigeration cycle. It determines the allowable value of the lower bound of the optimal pressure ratio. On the other hand, when the compression and expansion efficiencies are not high enough, $r_{Pm} \gg (r_P)_{\min}$ so that $r_{Pm}$ may be too large to be practical. In this case, the pressure ratio should not be required to be situated in the region determined by equation (18). In addition, it can be found by comparing curves b′ and c′ in figure 4 that the influence of the expansion efficiency on the coefficient of performance is more obvious than that of the compression efficiency.

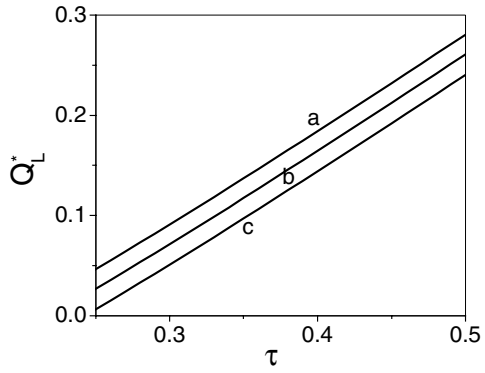


**Figure 7.** The $Q_L^*$–$\tau$ curves for given pressure $P_L = 0.5$ MPa and pressure ratio $r_P = 60$. The values of the parameters $T_H$ and $\eta_e$ are the same as those used in figure 2.

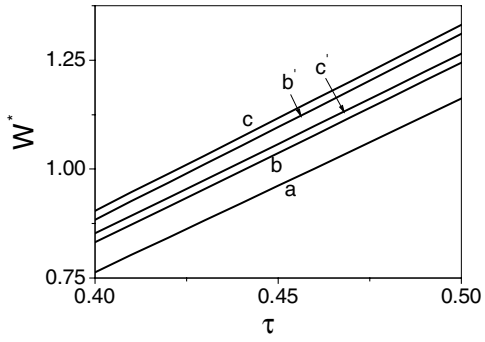


**Figure 8.** The $W^*$–$\tau$ curves for given pressure $P_L = 0.5$ MPa and pressure ratio $r_P = 60$. The values of the parameters $T_H$, $\eta_e$ and $\eta_c$ are the same as those used in figure 4.

It is seen from figure 6 that $R_{\mathrm{QL}}$ is always less than 1 and decreases quickly as the pressure ratio $r_P$ increases. This implies the fact that the refrigeration load of an irreversible quantum Bratyon refrigeration cycle working with a Fermi gas is always less than that of an irreversible classical Bratyon refrigeration cycle working with an ideal gas. The curves in figure 6 clearly show that the influence of quantum degeneracy on the relative refrigeration load $R_{\mathrm{QL}}$ increases as the expansion efficiency increases. When $\eta_e = 1$, the relative refrigeration load $R_{\mathrm{QL}}$ is only affected by the quantum degeneracy. In general, the relative refrigeration load $R_{\mathrm{QL}}$ is affected not only by the quantum degeneracy but also by the expansion efficiency. When the expansion efficiency is small, the influence of quantum degeneracy is not dominant so that there is a large relative refrigeration load because the refrigeration load of a classical Brayton cycle is also affected by the irreversibility of the expansion process.

Similarly, equations (13)–(16) can be used to plot the $Q_L^* \sim \tau$, $W^* \sim \tau$, $\varepsilon \sim \tau$ and $R_{\mathrm{QL}} \sim \tau$ characteristic curves of the cycle for given parameters $T_H$, $P_L$, $r_P$, $\eta_e$ and $\eta_c$, as shown in figures 7–10, respectively. It is clearly seen from the curves in figures 7–10 that the dimensionless refrigeration load $Q_L^*$ and work input $W^*$, coefficient of performance $\varepsilon$ (except for the case of $\eta_e = \eta_c = 1$) and relative refrigeration load $R_{\mathrm{QL}}$ are monotonically increasing functions of the temperature ratio $\tau$ of the two heat reservoirs for a set of given parameters $T_H$, $P_L$, $r_P$, $\eta_e$, and $\eta_c$. The curves in figures 7–10 also show that the larger the irreversibility in the cycle is, the smaller the dimensionless refrigeration load $Q_L^*$ and coefficient of performance

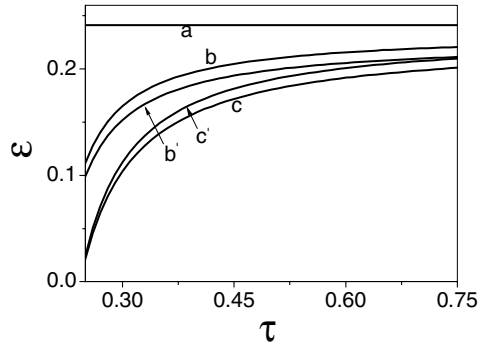


**Figure 9.** The $\varepsilon$–$\tau$ curves. The values of the parameters $P_L$, $r_P$, $T_H$, $\eta_e$ and $\eta_c$ are the same as those used in figure 8.

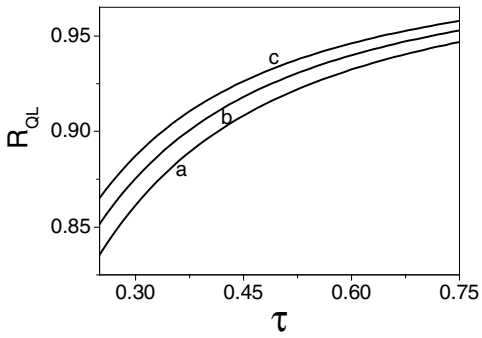


**Figure 10.** The $R_{\mathrm{QL}}$–$\tau$ curves. The values of the parameters $P_L$, $r_P$, $T_H$ and $\eta_e$ are the same as those used in figure 7.

$\varepsilon$, while the larger the dimensionless work input $W^*$ and relative refrigeration load $R_{\mathrm{QL}}$. This indicates that the influence of irreversibility in the working substance on the performance of the cycle is remarkable. Moreover, it can be seen from figure 9 that when $\eta_e$ and/or $\eta_c$ are smaller than 1, the coefficient of performance $\varepsilon$ is dependent not only on the pressure but also on the temperature, as shown in the curves b, b′, c and c′ in figure 9. This is different from the case of $\eta_e = \eta_c = 1$, in which the coefficient of performance is only dependent on the pressure, as shown in the curve a in figure 9. Figures 8 and 9 also show that for any value of $\tau$, the influence of the compression efficiency on the work input is more obvious than that of the expansion efficiency while the influence of the expansion efficiency on the coefficient of performance is more obvious than that of the compression efficiency.

## 5. Several special cases

It is significant to note that for some special cases, the results obtained above may be simplified.

### *5.1. Strong gas degeneracy*

Under the low-temperature and high-density conditions (i.e. the condition of strong gas degeneracy), the Fermi function can be expanded in powers of $\ln z$, i.e. [14]

$$f_n(z) = \frac{(\ln z)^n}{\Gamma(n+1)}\left\{1 + n(n-1)\frac{\pi^2}{6}\left(\frac{1}{\ln z}\right)^2 + n(n-1)(n-2)(n-3)\frac{7\pi^4}{360}\left(\frac{1}{\ln z}\right)^4 + \cdots\right\}. \tag{19}$$

Starting from equation (19), we can derive the first approximation of the correction function $F(z) = f_{5/2}(z)/f_{3/2}(z)$ as [2]

$$F(T, P) = \frac{2}{5}\frac{AP^{2/5}}{T} + \frac{\pi^2}{10}\frac{T}{AP^{2/5}}, \tag{20}$$

where $A = (15\pi^2\hbar^3)^{2/5}/(2km^{3/5})$. By using equation (20), equations (13)–(17) may be, respectively, simplified as

$$Q_L = \frac{Nk\pi^2}{4A}P_L^{-2/5}T_H^2(\tau^2 - X^2), \tag{21}$$

$$W = Q_H - Q_L = \frac{Nk\pi^2}{4A}P_H^{-2/5}T_H^2\left[(\tau Y)^2 - 1 - r_P^{2/5}(\tau^2 - X^2)\right], \tag{22}$$

$$\varepsilon = \frac{Q_L}{Q_H - Q_L} = \frac{r_P^{2/5}(\tau^2 - X^2)}{(\tau Y)^2 - 1 - r_P^{2/5}(\tau^2 - X^2)}, \tag{23}$$

$$R_{\mathrm{QL}} = \frac{Q_L}{Q_L^C} = \frac{\pi^2 T_L(\tau + X)}{10A\tau P_L^{2/5}} \tag{24}$$

and

$$r_P > (r_P)_{\min} = \left(\frac{\eta_e}{\eta_e + \tau - 1}\right)^{5/2}. \tag{25}$$

Equation (25) shows that the minimum pressure ratio $(r_P)_{\min}$ is only dependent on the temperature ratio of the heat reservoirs and expansion efficiency and independent of the compression efficiency because it is derived from equation (13).

### *5.2. Weak gas degeneracy*

Under the higher temperature and lower density condition (i.e. the condition of weak gas degeneracy), the Fermi function can be expanded [14]

$$f_n(z) = \sum_{l=1}^{\infty}(-1)^{l-1}\frac{z^l}{l^n} \tag{26}$$

and the first approximation of the correction function can be expressed as [2]

$$F(T, P) = 1 + BP/T^{5/2}, \tag{27}$$

where $B = (2\pi\hbar^2/m)^{3/2}/(4\sqrt{2}k^{5/2})$. By using equation (27), equations (13)–(16) can be, respectively, simplified as

$$Q_L = \frac{5}{2}NkT_H\left\{\tau - X + \left(\tau BP_L/T_L^{5/2}\right)[1 - (\tau/X)^{3/2}]\right\}, \tag{28}$$

$$\varepsilon = \frac{Q_L}{Q_H - Q_L} = \frac{\tau - X + \left(BP_L\tau/T_L^{5/2}\right)[1 - (\tau/X)^{3/2}]}{\tau Y - \tau + X - 1 + \left(\tau BP_L/T_L^{5/2}\right)[r_P(Y^{-3/2} - \tau^{3/2}) - 1 + (\tau/X)^{3/2}]}, \tag{29}$$

$$W = \frac{5}{2}NkT_H\left\{\tau Y - \tau + X - 1 + \left(\tau B P_L \Big/ T_L^{5/2}\right)[r_P(Y^{-3/2} - \tau^{3/2}) - 1 + (\tau/X)^{3/2}\right\}, \tag{30}$$

and

$$R_{\mathrm{QL}} = \frac{\tau - X + \left(\tau B P_L \Big/ T_L^{5/2}\right)[1 - (\tau/X)^{3/2}]}{\tau - X}. \tag{31}$$

It can be proved from equation (28) that equation (25) is still true in this case.

### *5.3. High-temperature limit*

When the temperature of the gas is high enough and its density is low enough, the fugacity of the gas $z$ is much smaller than unity. In such a case, $f_l(z) = z$, $F(T, P) = 1$ and an ideal Fermi gas becomes an ideal classical gas. Equations (13)–(16) can be, respectively, simplified as

$$Q_L = \frac{5}{2}NkT_H(\tau - X) \equiv Q_L^C, \tag{32}$$

$$W = \frac{5}{2}NkT_H(\tau Y - 1 - \tau + X), \tag{33}$$

$$\varepsilon = \frac{Q_L}{Q_H - Q_L} = \frac{\tau - X}{\tau Y - \tau + X - 1} \tag{34}$$

and

$$R_{\mathrm{QL}} = 1, \tag{35}$$

while equation (25) is also true. In this case, we can further calculate

$$r_{Pm} = \left(\frac{\eta_e + a}{\eta_e + \tau - 1}\right)^{5/2} \tag{36}$$

from equation (34), where $a = [\eta_e(\eta_c - \eta_c\eta_e + \tau - \eta_c\tau)(1/\tau - 1)]^{1/2}$.

### *5.4. $\eta_e = \eta_c = 1$*

When the irreversibility of two isentropic processes is negligible, $\eta_c = \eta_e = 1$. Equations (13)–(17) can be, respectively, simplified as

$$Q_L = \frac{5}{2}NkT_H\left[\tau F(T_L, P_L) - r_P^{-2/5}F(T_H, P_H)\right], \tag{37}$$

$$W = \frac{5}{2}NkT_H F(T_H, P_H)\left[\tau r_P^{2/5}\frac{F(T_L, P_L)}{F(T_H, P_H)} - 1\right]\left(1 - r_P^{-2/5}\right) = Q_L\left(r_P^{2/5} - 1\right), \tag{38}$$

$$\varepsilon = \frac{1}{r_P^{2/5} - 1}, \tag{39}$$

$$R_{\mathrm{QL}} = \frac{\tau r_P^{2/5}F(T_L, P_L) - F(T_H, P_H)}{r_P^{2/5}(\tau - X)} \tag{40}$$

and

$$r_P > (r_P)_{\min} = (f/\tau)^{5/2}, \tag{41}$$

where $f = F(T_H, P_H)/F(T_L, P_L)$. It is clearly seen from equation (39) that the coefficient of performance $\varepsilon$ is only a function of the pressure ratio $r_P$, which is the same as that of the Brayton refrigeration cycle using an ideal classical gas as the working substance.

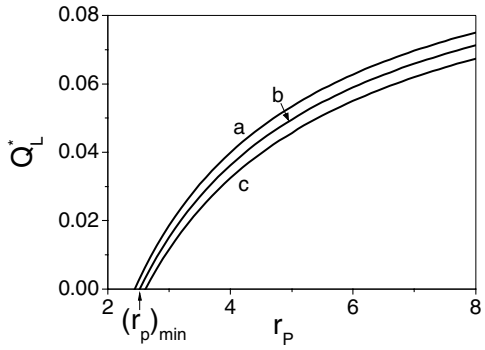


**Figure 11.** The $Q_L^*$–$r_P$ curves for given parameters $T_L = 210\,\mathrm{K}$, $T_H = 300\,\mathrm{K}$ and $P_L = 0.5\,\mathrm{MPa}$. Curves a, b and c correspond to the cases of $\eta_e = 1.00$, 0.97 and 0.94, respectively.

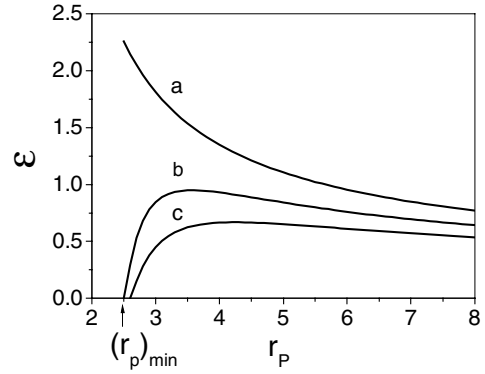


**Figure 12.** The $\varepsilon$–$r_P$ curves for given parameters $T_L = 210\,\mathrm{K}$, $T_H = 300\,\mathrm{K}$ and $P_L = 0.5\,\mathrm{MPa}$. Curves a, b and c correspond to the cases of $\eta_e = \eta_c = 1.00$, 0.97 and 0.94, respectively.

In the high temperature limit, $f = 1$. Consequently, the minimum pressure ratio, $(r_P)_{\min} = \left(r_P^c\right)_{\min} = \tau^{-5/2}$, can be derived from equation (41), where $(r_P)^c_{\min}$ is the minimum pressure ratio in the two constant-pressure processes of a classical Bratyon refrigeration cycle.

## 6. Discussion

It should be pointed out that the performance of a Fermi quantum refrigeration cycle is dependent on the choice of the working substance. However, using the above equations and same method, we can discuss the performance of the Fermi quantum refrigeration cycle working with other working substances, besides $^3$He. For example, when the ideal electron gas is used as the working substance, its quantum effect is still obvious at room temperatures. In such a case, the ideal electron gas is of strong degeneracy and the low-temperature and high-density conditions is still satisfied. Consequently, equations (20)–(25) may be directly used to discuss the performance of the refrigeration cycle working with an ideal electron gas. Thus, using equations (21) and (23), one can generate the $Q_L^* \sim r_P$ and $\varepsilon \sim r_P$ characteristic curves of the cycle for given parameters $T_L = 210$ K, $T_H = 300$ K and $P_L = 0.5$ MPa, as shown in figures 11 and 12. These curves in figures 11 and 12 clearly show that the performance characteristics of the cycle working with an ideal electron gas are similar to those

of the cycle using $^3$He as the working substance, although the values of the various parameters in the different refrigeration cycles are different from each other. If one considers the electron gas in a simple metal at room temperatures as the working substance, the pressures in the cycle are very large. Using the method mentioned above, one can obtain similar performance characteristic curves and results.

## 7. Conclusions

The influence of the quantum degeneracy of the Fermi gas and the irreversibility of the working substance in the cycle on the performance of the Brayton refrigeration cycle using an ideal Fermi gas as the working substance has been analysed in detail. Expressions for several important parameters are derived and some curves, which can reveal the performance characteristics of the cycle, are presented. It is found that the influence of the quantum degeneracy of the Fermi gas on the minimum pressure ratio is negligible, and consequently the minimum pressure ratio is determined by equation (25). However, the influence of the irreversibility of the working substance in the cycle on the minimum pressure ratio is remarkable. The larger the irreversibility is, the larger the minimum pressure ratio. Because of the influence of the quantum degeneracy, the refrigeration load of an irreversible Fermi quantum Bratyon refrigeration cycle is always less than that of an irreversible classical Bratyon refrigeration cycle. Moreover, the reasonably operating region of the pressure ratio and the various interesting problems of the cycle are discussed in detail. The results obtained here will be helpful to further understand the general performance characteristics of the Fermi Brayton refrigeration cycle.

## Acknowledgments

This work has been supported by the Key Project Foundation of Science and Technology Research of Ministry of Education, People's Republic of China.

## References

[1] Garrod C 1995 *Statistical Mechanics and Thermodynamics* (New York: Oxford University Press)
[2] Chen J, He J and Hua B 2002 *J. Phys. A: Math. Gen.* **35** 7995
[3] Chen J and Lin B 2003 *J. Phys. A: Math. Gen.* **36** 11385
[4] Scully M O 2002 *Phys. Rev. Lett.* **88** 050602
[5] Saygin H and Sisman A 2001 *J. Appl. Phys.* **90** 3086
[6] Lin B, He J and Chen J 2003 *J. Non-Equilib. Thermodyn.* **28** 176
[7] Lin B and Chen J 2003 *Open Sys. Inform. Dyn.* **10** 147
[8] Sisman A and Saygin H 1999 *J. Phys. D: Appl. Phys.* **32** 664
[9] Saygin H and Sisman A 2001 *Appl. Energy* **69** 77
[10] Rocco J M M, Velasco S, Medina A and Calvo Hernández A 1997 *J. Appl. Phys.* **82** 2735
[11] Sahin B, Kodal A, Yilmaz T and Yavuz H 1996 *J. Phys. D: Appl. Phys.* **29** 1162
[12] Medina A, Rocco J M M and Calvo Hernández A 1996 *J. Phys. D: Appl. Phys.* **29** 2802
[13] Gordon J M and Huleihil M 1992 *J. Appl. Phys.* **72** 829
[14] Pathria R K 1972 *Statistical Mechanic* (New York: Pergamon)
[15] Landau L D and Lifshitz E M 1980 *Statistical Physics* (London: Pergamon)